Published on 20 February 2025. Downloaded by Singapore University of Technology and Design on 2/25/2025 3:12:51 AM.

Journal of Materials Chemistry B

ROYAL SOCIETY OF CHEMISTRY

COMMUNICATION

View Article Online
View Journal

Check for updates

Cite this: DOI: 10.1039/d4tb02763a

Received 13th December 2024,
Accepted 18th February 2025

DOI: 10.1039/d4tb02763a

rsc.li/materials-b

A low-cost biocompatible and biodegradable multipurpose resistive ink for monitoring biological systems†

Akshayakumar Kompa,[a] Revathi Ravindran,[a] Jianyu Hao[a] and Javier G. Fernandez *[abc]

Flexible and biocompatible strain sensors are becoming increasingly important in fields such as health monitoring, wearable electronics, and environmental sensing because they offer significant advantages over conventional rigid systems. However, they lack the versatility and ecological and physiological biocompatibility necessary for broader integration within biological systems. Here, we describe the development of an inexpensive water-based plasticized chitosan–carbon black composite ink that can be used to produce conductive and biocompatible strain sensors. The ink can be applied to various surfaces, including skin, internal organs, and other biological tissues, using numerous methods, such as painting, dipping, and stamping. Furthermore, this unprecedented ability to attach and conform to biological surfaces allows the exploration of secondary sensing innovations, such as exploiting skin wrinkles to improve sensitivity. This study demonstrates that the ink exhibits a reliable change in electrical resistance in response to a wide range of motions, from subtle vibrations during speech and heartbeats to extensive articulations, like finger and elbow movements. This exceptional sensitivity range, biocompatibility, and the ink's low cost, biodegradability, and ease of removal enhance its applicability in sustainable, temporary, and customizable sensing solutions, highlighting its potential for versatile applications in human health monitoring, motion detection, and environmental sensing.

Introduction

The current "data age" is a transformative era in which the exponential growth of data is reshaping industries and everyday life, creating new opportunities for innovation, efficiency, and informed decision-making. This surge in data generation is fueled by the proliferation of sensors embedded in all sorts of products and devices, alongside recent advances in machine learning that have enabled the processing and analysis of these large data streams to identify trends and make predictions.

Flexible strain sensors are particularly rapidly evolving and have enabled the incorporation of movement analysis into soft and flexible materials, resulting in the development of new applications in emerging fields with broad and direct implications for human life, such as health monitoring, smart textiles, and soft robotics.[1] In addition to enabling entire new fields, these flexible and stretchable strain sensors have also shown themselves to be promising alternatives to traditional, rigid, metal-based or semiconductor-based sensors, providing better performance without the existing limitations of detection range or complex production processes.[2,3] It is therefore not surprising that, despite the very recent inception of these flexible sensors, even conservative estimates predict a global market size of more than $15 billion by 2032.[4]

Flexible strain sensors—like rigid ones—work by measuring physical changes in a material under stress. The most commonly used sensors are those based on changes in electrical resistance, which is easily measurable with simple and miniaturizable electronics.[5] Such sensors are usually made of synthetic polymers, either alone or as part of a composite with inorganic components, and the sole focus of their development has been on their sensing abilities and manufacturability.

However, the ability of flexible strain sensors to interact with curved and soft surfaces has sparked interest in developing biocompatible sensors for applications that require continuous but unobtrusive observation of biological systems, such as health and environmental monitoring.[6,7] Biopolymers, in particular, have been shown to be superior to their synthetic counterparts for such applications, but their biocompatibility comes with a high cost and narrow applicability, limiting their use to semi-permanent solutions for continuous monitoring in controlled environments. However, there are numerous other potential applications for temporary, flexible strain sensors in human health,[8,9] food safety,[10,11] and environmental monitoring,[12] which remain

[a] Engineering and Product Development, Singapore University of Technology and Design, Singapore
[b] Institute for Bioengineering of Catalonia, Barcelona, Spain. E-mail: jgomez@ibecbarcelona.eu
[c] ICREA, Barcelona, Spain

† Electronic supplementary information (ESI) available. See DOI: https://doi.org/10.1039/d4tb02763a

Published on 20 February 2025. Downloaded by Singapore University of Technology and Design on 2/25/2025 3:12:51 AM.

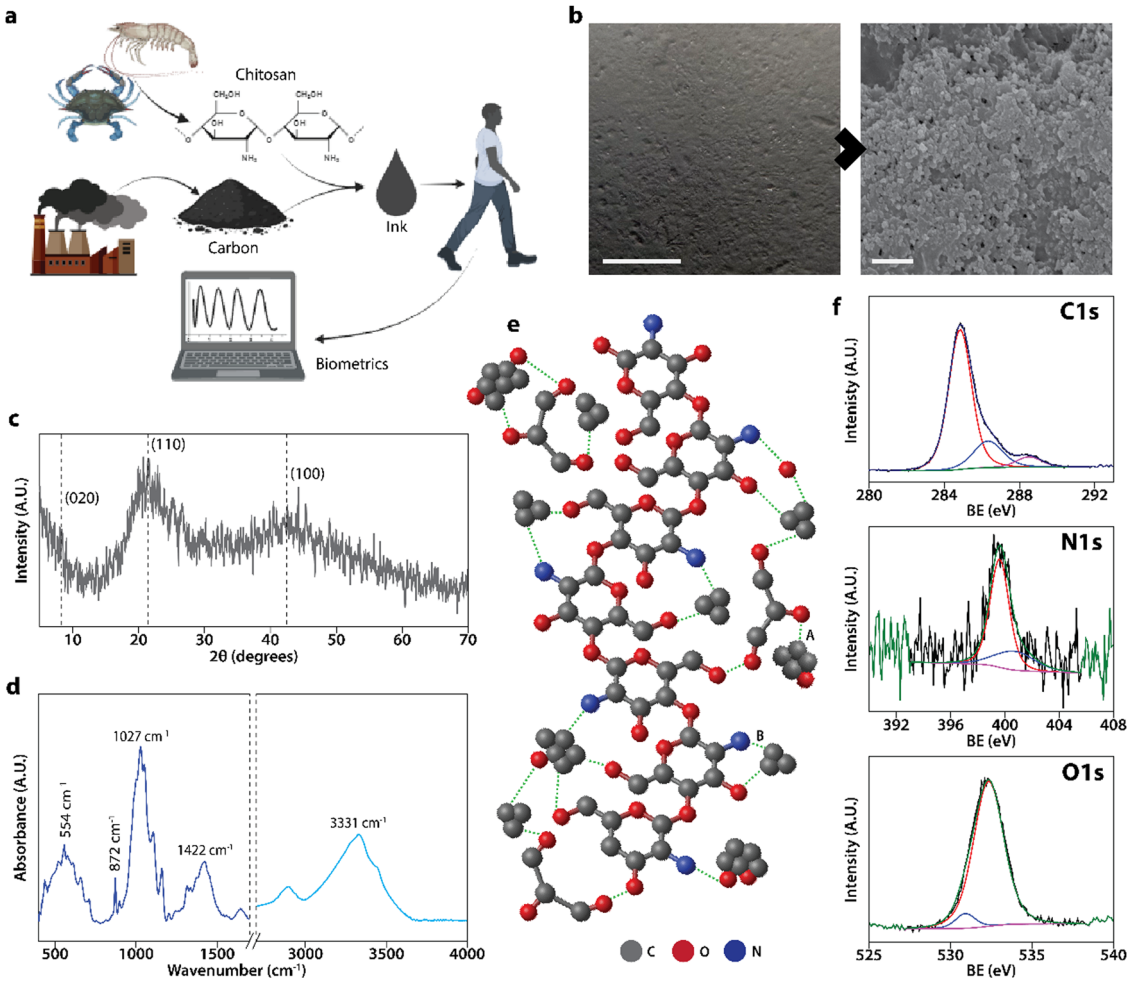


Fig. 1 Formation and molecular characterization of the resistive ink. (a) Diagram of the formation elements of the biocompatible resistive ink. The ink is made from chitosan (a byproduct of the processing of crustaceans by the fishing industry), carbon black (the product of natural or artificial incomplete combustion of organic matter), and glycerol. Both elements form a colloidal suspension in a water solution to create a liquid ink, which, upon vitrification, solidifies into a composite with variable resistance under stress. (b) Optical image (left) and scanning electron image (right) of the dry ink used during the experiments (3.7% w/v) where the carbon particles and their densely packed aggregation are clearly differentiated. Scale bars are 10 mm (left) and 0.001 mm (right). See Fig. S1 (ESI†) for other concentrations. (c) X-ray diffraction of the 3.7% carbon black ink. Two major peaks of chitosan and carbon black were observed at 20.6° and 42.6°, corresponding to the (110) and (100) planes, respectively. While the amount of chitosan and carbon black is very similar (1.2 times higher for carbon black), the disruption of the crystallization of chitosan by introducing carbon black makes the former dominate the spectrum, while most chitosan is present as an amorphous contribution. (d) Fourier-transform infrared spectrum of the ink, showing the interaction of functional groups of chitosan, carbon black, and glycerol. The interaction of carbon black with hydroxyl groups of chitosan and glycerol results in a shift of the major peaks with respect to the pure carbon black spectrum (Fig. S3, ESI†), while the presence of the carbonyl group is evidenced in the 1027 cm^{-1} peak. The strong C–C peak at 1648 cm^{-1} overshadows the amide groups of chitosan. (e) Diagram of the molecular interactions between chitosan, carbon black, and glycerol. Hydroxyl groups in chitosan and glycerol interact with carbon black, while aggregated carbon molecules also engage with amide and hydroxyl groups. (f) High-resolution XPS scans of dry carbon ink (3.7%). From top to bottom: C 1s, N 1s, and O 1s spectra and their deconvolutions. Refer to Fig. S4 (ESI†) for similar analyses of other ink compositions.

unexplored because current sensors lack simultaneous biodegradability, versatility, and cost-effectiveness.

Here, we demonstrate the production of a water-based ink comprising chitosan and carbon black nanoparticles and plasticied using glycerol that is intended for use in monitoring physiological movements (Fig. 1a). The conductive and versatile ink can be directly applied to various surfaces, including tissue (such as skin and muscle), cellulose, and other organic and inorganic materials. It can be applied using different methods like brush painting, pen drawing, or stamping, and can be easily removed with warm water. This ink's performance and ability to abruptly and rapidly change electrical resistance in response to movement is highly consistent. This allows it to monitor a wide range of physiological actions, from a beating heart to the vibrations of a throat while speaking, to the articulation of bones and joints. The latter is used, as an example, to record and virtually reproduce the movement of a hand. This ink stands out from other conductive inks on the market and from previous studies due to its unique combination of affordability, biodegradability, biocompatibility, and sensitivity (Table S1, ESI†).

 This journal is © The Royal Society of Chemistry 2025

Published on 20 February 2025. Downloaded by Singapore University of Technology and Design on 2/25/2025 3:12:51 AM.

The use of chitosan is not arbitrary; this biocompatible biopolymer exhibits mechanical characteristics that are similar to those of commodity plastics while also being both approved for medical use[13] and fully biodegradable in environmental conditions.[14] This biodegradability is essential to mitigate the accumulation of long-lasting materials in Earth's ecosystems that would otherwise result from applications for which recovery is not feasible.[15,16] Furthermore, chitin—in all its deacetylation forms, including chitosan—is the second most abundant natural biopolymer on Earth, surpassed only by cellulose. Indeed, while it is commonly harvested as a bioproduct from the processing of crustaceans in the fishing industry, it can also be produced and extracted locally from every ecosystem on the planet.[17] This is because it is synthesized and used in almost all biological kingdoms, from the walls of fungi to the exoskeletons and sensing organs of insects and mollusks[18] to the mucosa and electroreceptors of vertebrates.[19,20]

Chitosan is, however, an insulating material, and for its use in electrical applications, it must be associated with conductive particles.[21] The use of chitosan with pure metals has recently created a new type of biological metalworking, which uses the unparalleled ability of chitosan to bind and aggregate metallic particles at room temperature into very compact solids that exhibit the properties of the pure metal.[22] While chitin–metal composites have already shown promising conductivity and applicability in electronics, their use in producing low-cost temporary sensors has been restricted by the cost and potential impact of the metal component. Similarly, carbon nanomaterials, such as nanotubes, nanorods, fullerene, and graphene, have shown good performance in electrical applications, but their cost severely limits their generalizability.[1,6] Here, we use the inexpensive carbon black—a byproduct from the incomplete combustion of organic matter—as the filler in the chitosan matrix.[23] Even as the matrix provides the composite with its mechanical characteristics, so the carbon black filler provides electrical conductivity with an efficiency inversely proportional to the distance between the particles (*i.e.*, more conductive the closer they are).

Carbon black is a zero-dimensional nanomaterial that is characterized by a high surface area for its volume, and both the electrical resistance between particles and the chitosan polymer's aggregation of particles are driven by surface-to-surface interactions. We therefore hypothesized that carbon black would be particularly suitable for forming a composite material for sensing conformational changes, especially those involving low levels of stress. This is the condition in which a low volume of the particles—which set the baseline for conductivity—is critical for observing a change in resistance from the background value.[24]

Results and discussion

To create the water-soluble, biocompatible composite ink, we used chitosan extracted from shrimp shells dissolved at a 3% concentration in a weak solution of acetic acid (1%; for comparison, table vinegar is 5–8%). Due to the hydrophobic surface of carbon black particles, they do not disperse naturally within water-based solutions; glycerol was therefore used as a natural and biocompatible dispersant.[25] In addition to its dispersive properties, glycerol acts as a plasticizer for chitosan, improving the dry ink's elasticity to match soft tissue (*e.g.*, skin).[26]

The chitosan/glycerol/carbon black mixture was sonicated for 10 minutes to break the particle aggregates. It has been demonstrated that the concentration of particles in a chitometallic composite strongly affects its mechanical and electrical properties;[22] to explore the effect of particle concentration, we therefore produced three samples within a pre-established range of concentrations that we have previously observed to produce positive results. Qualitatively, the low-loading samples (1.9% w:v) were characterized by outstanding mechanical properties and rubber-like flexibility but poor conductivity, while at the other extreme of the viable range, the high-loading samples (5.5% w:v) resulted in brittle composites that tended to crack when dried (Fig. S1, ESI†). To explore practical uses, we therefore used a composite between the extremes (3.7% w:v) that showed a balance of mechanical and electrical requirements, suitable for both low- and high-strain sensing and with minimal cracks under load.

Molecular characterization

At the molecular scale, the concentration of carbon particles was observed to influence the ability of chitosan to crystalize. X-ray diffraction patterns of the different composites showed that chitosan always precipitated in the same crystal configuration (Fig. 1c and Fig. S2, ESI†). However, with increasing amounts of carbon black hindering the process, the number of organized molecules decreased, resulting in more amorphous materials. Unexpectedly, at low concentrations of carbon black, the particles tended to make aggregates, while at high concentrations, they showed a uniform distribution (Fig. 1b and Fig. S1, ESI†). This might appear counterintuitive but is a result of the emulsifying function of the glycerol. The dispersion of the particles during sonication is driven by internal frictions[27] and benefits from higher particle concentrations. Under normal conditions, the dispersion process is balanced by the tendency of the particles to reestablish surface interaction and to aggregate again—a process that also benefits from large particle concentrations.[28] While glycerol does not contribute to the dispersion process, it blocks the particles' active groups immediately after they become available, effectively preventing interaction with other particles and thus the formation of clusters.

The highest of the previously tested concentrations of conductive particles (5.5% w:v) resulted in improved electrical conduction through the dried colloidal suspension/ink but also led to the formation of macroscopic cracks under minimal stress (Fig. S1, ESI†), which ultimately resulted in the loss of electrical conductivity. In contrast, the 3.7% concentration showed a uniform distribution of the particles without the disadvantage of macroscopic cracks, yet a more in-depth

Published on 20 February 2025. Downloaded by Singapore University of Technology and Design on 2/25/2025 3:12:51 AM.

analysis revealed a surface riddled with microscopic cracks (Fig. 1b). Unlike the cracks in the highest concentration sample, these microcracks were not deep or long enough to prevent electrical conductivity. Indeed, we hypothesized that they might actually contribute to the material's excellent results and broad sensitivity range, particularly at low strains, as the changes in conductivity would then be due mainly to the opening and closing of the gaps created by the cracks rather than the relative separation of the particles embedded in the material—the latter being the main contributor at high strains. Interestingly, using a variable gap in a chitinous structure to sense strains and vibrations is the main principle of the slit sensilla in the cuticles of scorpions and spiders.[29]

The molecular interactions and structure of the chitosan, carbon black, and glycerol colloidal suspensions are shown in Fig. 1e. An infrared analysis (Fig. 1d and Fig. S3, ESI†) of dried ink shows dominant peaks for the stretching of –OH (due to an adsorbed water/hydroxyl group on the carbon black surface), the bending vibration of –CH, and the stretching vibration of –CO.[30] The sterically available hydroxyl groups on the surface of carbon black nanoparticles can form hydrogen bonds with similar groups on chitosan molecules; as discussed above, the interactions between the hydroxyl groups and the carbon black particles must compete with glycerol, which is a small molecule of high mobility. The effect of glycerol can therefore be observed as a red shift in the –OH stretching peak position, from 3253 cm^{-1} to 3336 cm^{-1}.

The interaction of the carbon black particles with the hydroxyl groups of the chitosan and glycerol is also accompanied by additional C–O bonds, observed in the FTIR spectra as a 1027 cm^{-1} peak.[31] Furthermore, adding glycerol to the chitosan solution results in an amide II band shift from 1541 to 1563 cm^{-1} (Fig. S4, ESI†), confirming an interaction through the primary amino group (C2). However, an interaction in the same locus with the carbon black particles could not be determined because the amide band is overshadowed by the overlapping C–C/C–O stretching peak from the particles (1648 cm^{-1}, position A in Fig. 1e).[32] This molecular information is supported by similar observations in the lower fingerprint region of the FTIR (400–1000 cm^{-1}), where the C–O stretching band at 560 cm^{-1} corroborates the interaction between the carbon black particles and the oxygen of hydroxyl groups. Similarly, the sharp peak at 874 cm^{-1} adjacent to the –OH wagging vibration (894 cm^{-1}) is characteristic of the C–N/C–C stretching vibration (position B in Fig. 1e) and is therefore consistent with the possible interaction between the carbon particles and the amine group of the chitosan, which again cannot be unequivocally corroborated due to the overlap with the particle–particle interactions. The redshift of the C–H stretching band in the chitosan (from 1407 cm^{-1} to 1425 cm^{-1}) after adding the carbon black confirms that the vitrification of the colloidal suspension into a solid ink is not driven solely by a physical entrapment of the carbon particles and that strong intermolecular interactions play a part in the process.[33]

An X-ray photoelectron spectroscopy (XPS) analysis also supported the molecular interactions identified by infrared spectroscopy (Fig. 1f and Fig. S4, ESI†). The deconvoluted high-resolution C 1s spectrum of dried ink shows three peaks at 284.79, 286.56, and 288.55 eV, which are attributable to C–(H, C), C–(O, N), and O–C–O/C═O, respectively.[31,34] The first peak corresponds to single-bonded carbon atoms (C–C) and C–H groups of chitosan, while the second broad peak corresponds to carbon atoms linked to the hydroxyl group (C–O). This second peak, therefore, confirms the interaction between the carbon black particles and the amide group of the chitosan, which, as mentioned, could not be resolved using infrared spectroscopy. This interaction is also observed in the N 1s spectrum, where the formation of new C–N bonds is unequivocally identified by the 401.6 eV peak.[35] The formation of hydroxyl bonds between carbon black and glycerol—to the detriment of the bonding between separate carbon black particles—is also evidenced by the 286.29 eV peak in C 1s and the 533.47 eV peak in O 1s.[35] This corroborates the transition from a conglomerate of carbon black particles to a dispersed and profusely connected colloidal suspension of carbon black, chitosan, and glycerol.

Consistent with the molecular and supramolecular analysis of the composite, its thermal degradation shows that the introduction of carbon black results in greater susceptibility of the chitosan to such degradation (Fig. S5, ESI†), which is in accordance with the amorphous configuration of the biopolymer. The decomposition temperature of the chitosan in the 3.7% carbon back composite is as low as 166 °C, in contrast to 260 °C for more crystalline pure chitosan. The amorphous phase is also characterized by a significantly higher water content, which in pure chitosan is 11.03% but increases to 19.51% for the 3.7% carbon black composite.

Applications

All the components that form the water-based colloidal suspension are biodegradable and biocompatible in both the environmental and biomedical senses and are thus appropriate for applications in which such biocompatibility is required. However, beyond the suitable chemical characteristics, the monitoring of human health and biological systems requires sensors that can conform to and connect with the complex curved surfaces that characterize organisms while still being able to sense movements ranging from mere vibrations (*e.g.*, heart, lungs, larynx) to large strains (*e.g.*, limb movements).[36] A sensitivity plot (*i.e.*, gauge factor; see Fig. 2a) of the dry ink demonstrates its ability to conform to this complex set of characteristics, with GF values of 9.47 and 17.18 (linear fitting, R^2 = 0.98) at low and high strains, respectively, enabling sensitivity to human motion that is vastly superior to both rigid sensors and costly and non-biodegradable flexible inks (Fig. 2b).[37–43]

There is a significant gap between the theoretical performance of the ink and its practical use, which is conditioned on factors that vary and are difficult to measure, such as applicability, affinity to different surfaces, and responses to complex movements. To demonstrate the potential applications of the ink, we therefore sought to evaluate its performance in several

 This journal is © The Royal Society of Chemistry 2025

Published on 20 February 2025. Downloaded by Singapore University of Technology and Design on 2/25/2025 3:12:51 AM.

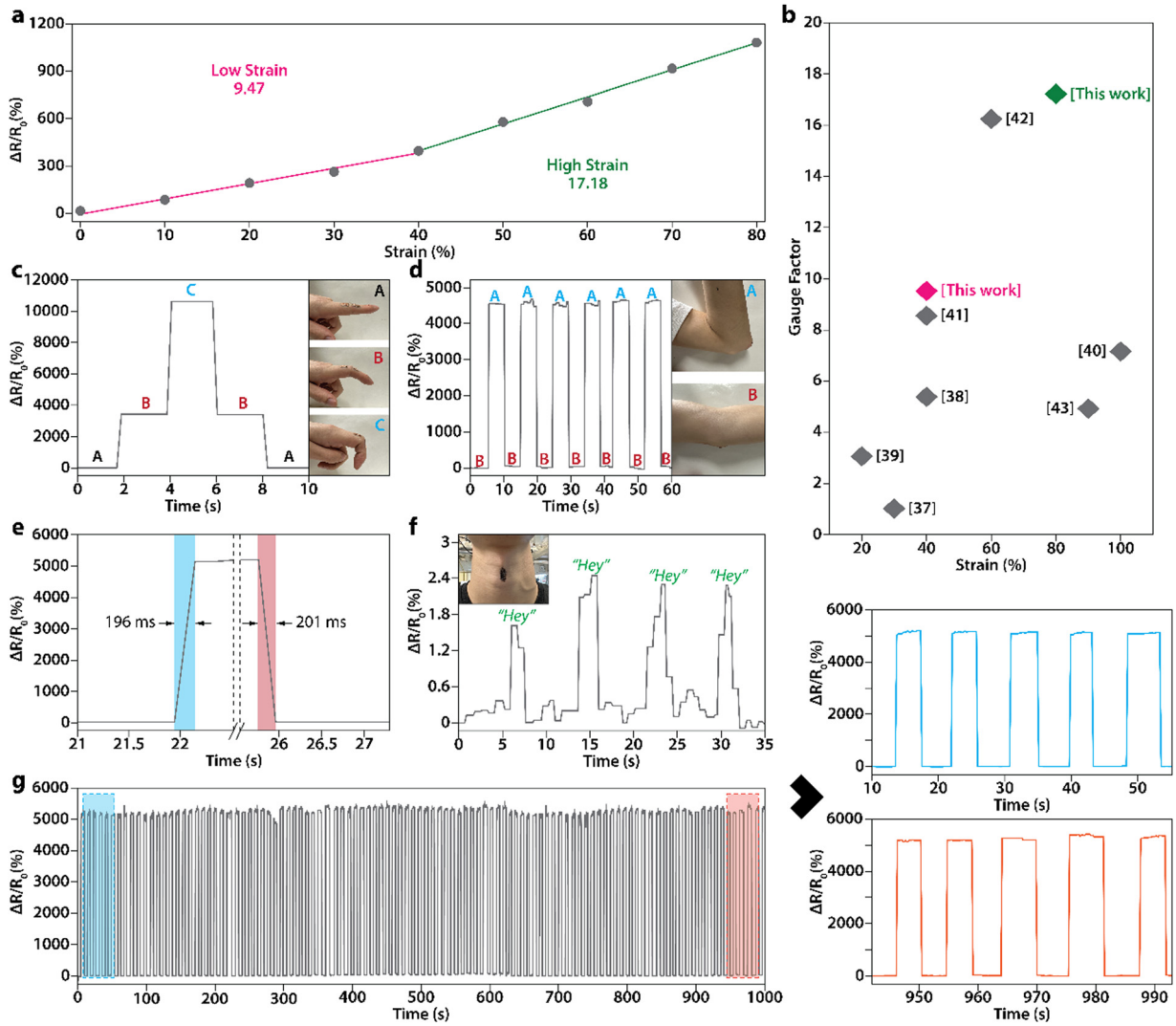


Fig. 2 Resistive properties and application of the bioink. (a) Sensitivity (gauge factor) determination for low and high strain values indicates that the 3.7% carbon black-loaded sample exhibits two differentiated linear fittings. These fittings are characteristic of an inflection point in the material's response to strain, enabling the separate detection of low and high strains (see Fig. S7 for the dependence of the sensitivity with the ink thickness and Fig. S8 for mechanical characterization, ESI†). (b) The gauge factor indicates the magnitude of the electrical resistance change of the material in response to strain. In the panel, the response of the resistive bioink under low and high strain is compared to state-of-the-art materials, showcasing significantly higher sensitivity in addition to its unprecedented range and versatility (see Table S1 for further comparison with existing products, ESI†). (c) Relative change in electrical resistance of a resistive ink painted on the index finger as it transitions between three positions (see Video S1 for further details, ESI†). (d) Elbow motion recorded as changes in electrical resistance during full contraction and expansion of the arm, including holding positions for several seconds to determine the articulation's movement (*i.e.*, dynamic) and state (*i.e.*, static). (e) Electrical resistance across a painted line on the skin measured during rapid wrist movements. (f) Ink applied on the throat and the electrical resistance in response to speech (see Video S2 for further information, ESI†). (g) Durability and reliability test of the ink painted on skin by bending and relaxing the wrist for 1000 seconds. At the right are close-up images of the recorded signal at the experiment's beginning (top, blue) and end (bottom, red).

real-world scenarios. To test its use in tracking body functions, we prepared comprehensive strain-sensing tests by applying the ink using a paintbrush to a test subject's wrist, finger, elbow, and throat (Fig. 2c–f and Video S1, ESI†). The ink was allowed to dry for 10 minutes before testing, and the subject's movements were recorded as changes in resistance using a multimeter connected to the two ends of the painting by copper wire.

The first test was performed by painting a thin line (~5 mm wide) on the top of the index finger, covering both the proximal and distal interphalangeal joints. The resistance was recorded as a function of the finger bending at different angles and demonstrated a linear and steady response, enabling the unequivocal differentiation between different bending angles (Fig. 2c). This steady and precise response would also enable much more advanced use of the data than simple monitoring, such as communication by Morse code using the position of the ink-marked finger (Fig. S5, ESI†). However, it is important to note that the current research focuses on developing the ink and evaluating its capabilities; no data processing has been attempted, and all signals are recorded and used exactly as

Published on 20 February 2025. Downloaded by Singapore University of Technology and Design on 2/25/2025 3:12:51 AM.

captured by a commercial multimeter to show the raw capabilities of the ink rather than its full potential for complex measurements and tasks.

The ink was then applied to the elbow to test large movements (Fig. 2d). Despite the different sizes and movement ranges, the results were similar to those observed for the fingers, with a consistent and measurable response after several cycles of bending and extending the arm. While the speed of response to any change in resistance is dependent mostly on the measuring tool and the speed of the movement itself rather than to the material employed, there was nevertheless a transition of less than 0.2 seconds between full extension and full contraction of the arm and measurement of the corresponding resistance values, reflecting the lack of ink-related bottlenecks in the measuring speed (Fig. 2e). Interestingly, for both the elbow and finger, the sensor sensitivity was two to three orders of magnitude higher than measurements performed on other body parts (*e.g.*, neck). While initially attributed to the relatively long range of the movements, this increased sensitivity was also observed in movements of much smaller amplitudes but performed on wrinkled skin, such as the horizontal displacement of the metacarpophalangeal joints

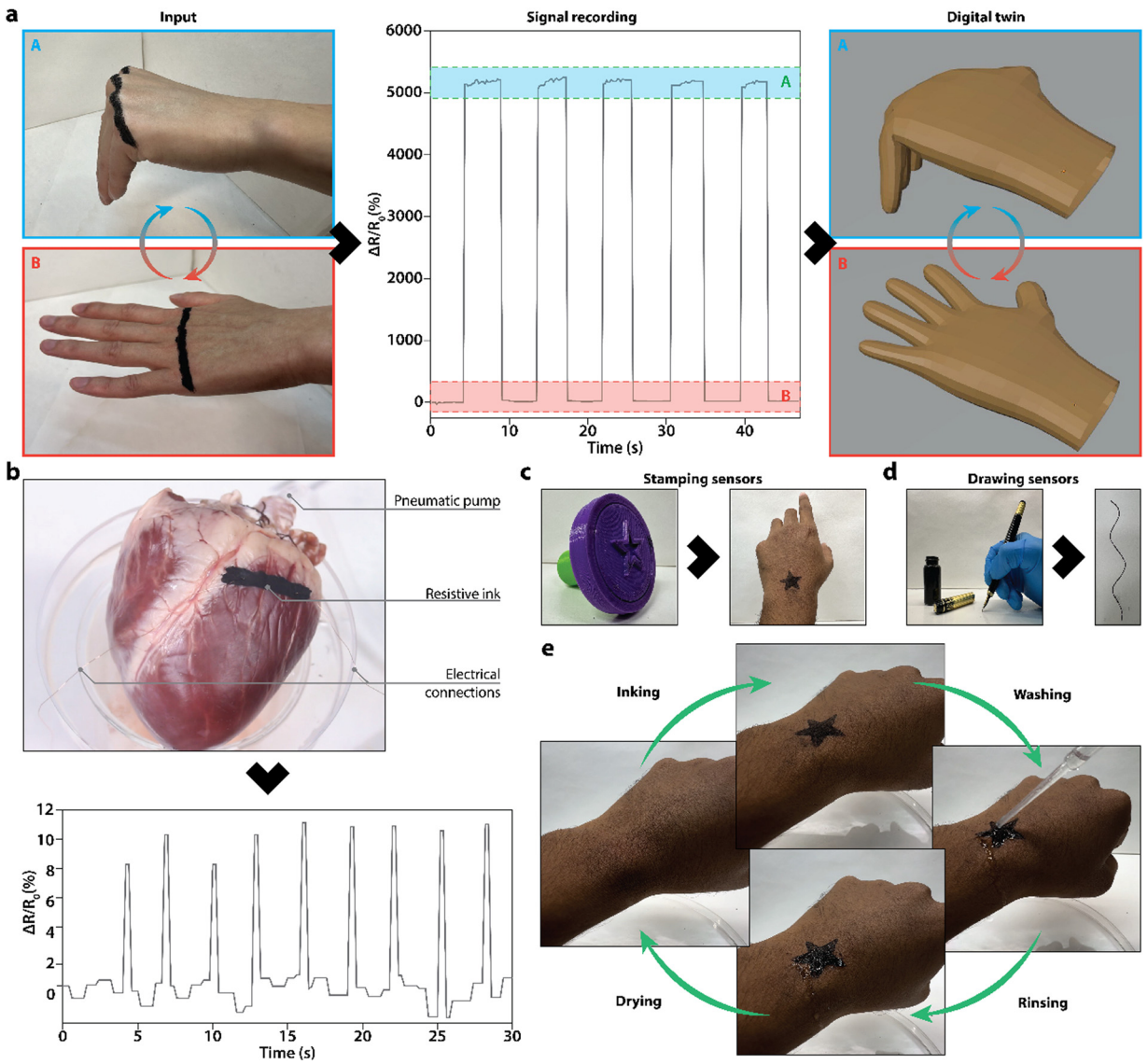


Fig. 3 Applications carbon ink and its degradation. (a) Biological ink painted on the knuckle and the recording of the electrical resistance to create a digital twin of the hand (see Video S3 for further information, ESI†). (b) Painting of a resistive line on the surface of a heart and recording of the simulated palpitation as changes in the electrical resistance across the extremes (see Video S4 for further information, ESI†). (c) 3D stamp used to apply a custom shape resistive sensor in predefined shapes. (d) Production of resistive sensors by loading the biological ink in a fountain pen, enabling the rapid production of inexpensive and environmentally friendly strain sensors, such as paper-based electronics. (e) Example of the removal of a resistive sensor on skin using warm water. Adding to the low cost and biodegradability, easily applying and removing the ink enables a generalizable use as a disposable alternative for short-term applications or when the sensor cannot be recovered. See Video S5 (ESI†) for water-resistant applications and medical wearables.

 This journal is © The Royal Society of Chemistry 2025

Published on 20 February 2025. Downloaded by Singapore University of Technology and Design on 2/25/2025 3:12:51 AM.

(*i.e.*, knuckles) during finger extensions. We hypothesize that, similar to the macroscopic cracks reported above, the extraordinary conformability of the ink to the wrinkled surface of the skin during articulations creates greater sensitivity by effectively using the expansion and contraction of the skin wrinkles themselves, similar to how arachnids use the slit sensillum, which inspired the fabrication of ultra-sensitive micro-crack-shaped strain sensors.[44,45] While wrinkles greatly enhanced the ink's sensitivity to movement—particularly over a relatively long range—the test of the ink on the throat to record neck movement and larynx vibrations during speech demonstrated that even low-amplitude movements are measurable without the need for secondary topographies (Fig. 2f and Video S2, ESI†).

Finally, the durability of the ink was tested over 1000 seconds of continuous bending and relaxing the wrist (Fig. 2g). No significant change in the output signal was observed, highlighting the ink's suitability for the measurement of repetitive physical movements.

During this study, we have emphasized the sensor's flexibility and ability to conform to complex shapes—even to natural skin wrinkles—for enhanced sensing mechanisms. However, due to its simplicity and to the lack of the multilayered structure that characterizes most flexible sensors, it can be uniquely applied as an ink instead of a prefabricated sensing element. This offers further versatility of application and customizability to very specific use scenarios, such as the isolation of complex movements. For example, the ink application to the knuckles enabled accurate monitoring of the finger positions without applying ink to the fingers themselves—information that was then used to create a digital twin of the hand state in a virtual environment (Fig. 3a and Video S3, ESI†). The animation seamlessly synchronized with the real-time movements of the hand, illustrating the capabilities of these flexible sensors to track and interpret complex motions and providing a new versatility to create distance between what we want to measure (*e.g.*, finger position) and what we can measure (*e.g.*, knuckle wrinkles). A similar test of the ability to monitor complex biological movements was performed using an *ex vivo* heart, in which the systole and diastole cardiac cycle was reproduced using a purpose-built auxiliary hydraulic pump attached to the left atrium (Fig. 3b and Video S4, ESI†). The composite ink was painted on the left side of the heart, and the expansion/contraction was recorded as a variance in the ink resistance, producing a clear "cardiogram" in which a signal similar to the QRS complex was observed.[46]

For consistency in this study, we applied the ink to the various surfaces—thus creating the sensors—using a paintbrush, which would be possible on almost any surface, irrespective of roughness or hardness. We also focused on painting on the surface of organs—including the skin—due to their complexity and clear use cases. There are, however, few theoretical or practical limitations to applying the ink using other methods (*e.g.*, inkjet printing, dipping, spraying) or to other surfaces (*e.g.*, paper, cartons, fruits, vegetables, clay, construction materials) suitable for water-based inks. For example, using a stamp and ink pad—spreading the resistive ink across the face of the stamp and transferring it to the target surface—would minimize calibration for applications not requiring versatility (Fig. 3c). Similarly, loading a fountain pen with resistive ink would allow sensors to be directly written, similar to painting with regular ink (Fig. 3d). Indeed, while the overall resistance of the sensor as a whole can be tuned by its pattern, we did not observe any significant differences in the sensing capabilities of the ink due to the application method.

In addition to the direct application of the ink on tissues, its water-based chemistry and compatibility with a wide range of biomaterials—not limited to tissues—enable its combined use with other biocompatible technologies to explore further applications. For instance, the ink can be used in wearables, transforming standard bandages and other medical products into "smart" devices capable of sensing movement. Furthermore, although the ink is intended for low-cost, temporary applications requiring water solubility and rapid biodegradability, combining it with other technologies can facilitate its adaptation to other conditions. This includes use alongside standard waterproof protections and composites for longer, more durable applications (Video S5, ESI†).

Conclusion

In conclusion, in this paper, we have reported a new type of water-based resistive ink with strong affinity for biological materials that allows a wide variety of surfaces to be transformed into pressure/strain sensors by direct application (*i.e.*, without support), including skin, internal organs, and other biological materials. The low—around $38 per liter—estimated cost of the ink, its fully biological composition and biodegradability (Fig. S6, ESI†), its easy applicability using a wide variety of methods, and its ability to be easily removed with warm water (Fig. 3e) make it an unprecedentedly sustainable and affordable alternative to existing flexible sensors. Furthermore, the ubiquitous nature of the ink's components and their existing industrial-scale production should enable the scaling up of resistive inks for generalized use in sensing applications—unrestricted by the production costs and recovery needs of current strain sensors—and its application to a broad range of areas, from health and environmental monitoring to motion capture and smart clothing.

Despite its high-level simplicity, the ink demonstrated unprecedented range and sensitivity at both low and high strains and proved effective in recording movements from simple vibrations to full-amplitude limb movements when applied directly to the skin. The conformability of the ink to the topography of the skin at the microscale—making it *de facto* a resistive skin—will enable the exploration of complex sensing mechanisms, such as the use of secondary topographies (*e.g.*, skin wrinkles) to improve the sensing range. We believe these results represent a new approach to developing sensors that is centered on general, customizable, and temporary use and is based on simple and ecologically integrated chemistry. We further believe that this approach will enable new uses and previously impossible applications, particularly involving biological systems.

Published on 20 February 2025. Downloaded by Singapore University of Technology and Design on 2/25/2025 3:12:51 AM.

Author contributions

AK and JGF conceived the idea of creating the resistive ink. AK performed the physical characterizations and aplciations with the assistance of JH. RR developed the virtual hand model and its integration with the signal recording. JGF and AK wrote the first draft of the article. All authors contributed to writing the manuscript.

Conflicts of interest

The technology described in this document and its applications are part of a patent application in which AK and JGF are inventors.

Acknowledgements

The authors thank Dr Cedric Finet from the National University of Singapore (NUS) for his assistance with the XPS analysis.

References

1 K. Dai, K. Zhou, C. Liu and C. Shen, Flexible conductive polymer composites for smart wearable strain sensors, *SmartMat*, 2020, **1**, 1010.
2 S.-H. Bae, Y. S. Rim, H. Chen, N. D. Marco and Y. Yang, Recent Progress in Materials and Devices toward Printable and Flexible Sensors, *Adv. Mater.*, 2016, **28**, 4415–4440.
3 M. Petrelli, B. Shkodra, A. Falco, M. A. C. Angeli and S. Vasquez, From Rigid to Flexible: Solution-Processed Carbon Nanotube Deposition on Polymeric Substrates for the Fabrication of Transistor-Based Ion Sensors, *IEEE J. Flexible Electron.*, 2023, **2**, 300–307.
4 Y. Luo, *et al.*, Technology Roadmap for Flexible Sensors, *ACS Nano*, 2023, **17**, 5211–5295.
5 H. Banerjee, H. Souri, A. Jusufi, N. Radacsi, A. A. Stokes, I. Park, M. Sitti and M. Amjadi, Wearable and Stretchable Strain Sensors: Materials, Sensing Mechanisms, and Applications, *Adv. Intell. Mater.*, 2020, **2**, 2000039.
6 M. Wang, G. Wang, M. Zheng, S. Yao and B. Ebo, High-Sensitivity GNPs/PDMS Flexible Strain Sensor with a Microdome Array, *ACS Appl. Electron. Mater.*, 2022, **4**, 4576–4587.
7 J. Li, X. Wang, H. Song, H. Huang and J. Gou, Highly Stretchable and Wearable Strain Sensor Based on Printable Carbon Nanotube Layers/Polydimethylsiloxane Composites with Adjustable Sensitivity, *ACS Appl. Mater. Interfaces*, 2018, **10**, 7371–7380.
8 Y. Yuan, B. Liu, H. Li, M. Li, Y. Song, R. Wang, T. Wang and H. Zhang, Flexible Wearable Sensors in Medical Monitoring, *Biosensors*, 2022, **12**, 1069.
9 M. Cheng, G. Zhu, F. Zhang, W.-L. Tang, S. Jianping, J.-Q. Yang and L.-Y. Zhu, A review of flexible force sensors for human health monitoring, *J. Adv. Res.*, 2020, **26**, 53–68.
10 S. K. Biswas, M. S. Islam, F. Jia, Y. Cao, Y. Li and C. Cao, Flexible Biosensors for Food Pathogen Detection, *Adv. Electron. Mater.*, 2024, **10**, 2300898.
11 W. Huang, X. Wang, J. Xia, Y. Li, L. Zhang, H. Feng and X. Zhang, Flexible sensing enabled agri-food cold chain quality control: A review of mechanism analysis, emerging applications, and system integration, *Trends Food Sci. Technol.*, 2023, **133**, 189–204.
12 Y. Yang and Z. D. Deng, Stretchable sensors for environmental monitoring, *Appl. Phys. Rev.*, 2019, **6**, 011309.
13 K. J. Tracy, B. Rukmanikrishnan and J. G. Fernandez, Secondary Reorientation and Hygroscopic Forces in Chitinous Biopolymers and Their Use for Passive and Biochemical Actuation, *Adv. Mater. Technol.*, 2023, **8**, 2300639.
14 D. E. Ingber and J. G. Fernandez, Manufacturing of Large-Scale Functional Objects Using Biodegradable Chitosan Bioplastic, *Macromol. Mater. Eng.*, 2014, **299**, 932–938.
15 F. Liu, Z. Shen, S. Huang, H. Wang, C. Yang, T. Hang, J. Tao, W. Xia and X. Xie, Progress of flexible strain sensors for physiological signal monitoring, *Biosens. Bioelectron.*, 2022, **211**, 114298.
16 Z. Wang, T. Yan and Z.-J. Pan, Flexible strain sensors fabricated using carbon-based nanomaterials: A review, *Curr. Opin. Solid State Mater. Sci.*, 2018, **22**, 213–228.
17 N. D. Sanandiya, C. Ottenheim, J. W. Phua, A. Caligiani, S. Dritsas and J. G. Fernandez, Circular manufacturing of chitinous bio-composites via bioconversion of urban refuse, *Sci. Rep.*, 2020, **10**, 4632.
18 B. A. Stankiewicz and R. A. Steinbrecht, Molecular composition of the wall of insect olfactory sensilla—the chitin question, *J. Insects Physiol.*, 1999, **45**, 785–790.
19 W. J. Tang, J. G. Fernandez, J. J. Sohn and C. T. Amemiya, Chitin Is Endogenously Produced in Vertebrates, *Curr. Biol.*, 2015, **25**, 897–900.
20 M. Phillips, W. J. Tang, M. Robinson, D. O. Daza, K. Hassan, V. Leppert, L. S. Hirst and C. T. Amemiya, Evidence of chitin in the ampullae of Lorenzini of chondrichthyan fishes, *Curr. Biol.*, 2020, **30**, R1254–R1255.
21 W. Wang, B. Zhang, D. Zhang, T. Li, H. Zhang, C. Du, W. Zhao and Y. Yang, A highly sensitive and stretchable strain sensor based on a wrinkled chitosan-multiwall carbon nanotube nanocomposite, *J. Mater. Chem. C*, 2021, **9**, 14848–14857.
22 S. Ng, G. Z. B. Ng, R. E. Simpson and J. G. Fernandez, A Biological Approach to Metalworking Based on Chitinous Colloids and Composites, *Adv. Funct. Mater.*, 2024, 2406800.
23 F. Wu, Y. Liu, X. Zhao and M. Liu, High-Performance Strain Sensors Based on Spirally Structured Composites with Carbon Black, Chitin Nanocrystals, and Natural Rubber, *ACS Sustainable Chem. Eng.*, 2018, **6**, 10595–10605.
24 S. H. Chang and M. A. U. Khalid, Flexible strain sensors for wearable applications fabricated using novel functional nanocomposites: A review, *Compos. Struct.*, 2022, **15**, 115214.
25 N. Okamoto, A. N. Nguyen, R. Abe, A. D. M. Heriyanto, N. Kumari, G. Pado, S. Tanimura, Y. Cho, M. Pandey, H. Benten and M. Nakamur, Carbon Nanotube Yarns Tailored Using Dispersants and Surfactants for Flexible and Wearable Thermoelectric Generators, *ACS Appl. Nano Mater.*, 2024, **7**, 9880–9886.

 This journal is © The Royal Society of Chemistry 2025

Published on 20 February 2025. Downloaded by Singapore University of Technology and Design on 2/25/2025 3:12:51 AM.

26 R. Adhikari, H. Liu, Q. Guo and B. Adhikari, Preparation and characterization of glycerol plasticized (high-amylose) starch–chitosan films, *J. Food Eng.*, 2013, **116**, 588–597.
27 C. Xu, Y. Wang, T. Jahnke, W. Verestek, S. Schmauder and J. P. Spatz, Microstructural Modeling and Simulation of a Carbon Black-Based Conductive Polymer–A Template for the Virtual Design of a Composite Material, *ACS Omega*, 2022, **7**, 28820–28830.
28 Y. Lu, L. Zhu, Y. Wang, L. Zhang and W. Wang, Preparation and characterization of dopamine-decorated hydrophilic carbon black, *Appl. Surf. Sci.*, 2012, **258**, 5387–5393.
29 L. Liu, Z. Han, J. Zhang, Q. Han, K. Wang, H. Song, Z. Wang, Z. Jiao, S. Niu and L. Ren, High-performance flexible strain sensor with bio-inspired crack arrays, *Nanoscale*, 2018, **10**, 15178–15186.
30 H. Zheng, Y. Liu and M. Liu, High performance strain sensors based on chitosan/carbon black composite sponges, *Mater. Des.*, 2018, **141**, 276–285.
31 B. Gieroba, *et al.*, Spectroscopic studies on the temperature-dependent molecular arrangements in hybrid chitosan/1,3-β-D-glucan polymeric matrices, *Int. J. Biol. Macromol.*, 2020, **159**, 911–921.
32 L. Zhou, X. Tang, Z. Le, Y. Wang, Z. Liu, G. Huang and A. A. Adesina, Preparation of porous chitosan/carboxylated carbon nanotube composite aerogels for the efficient removal of uranium(VI) from aqueous solution, *Int. J. Biol. Macromol.*, 2020, **160**, 1000–1008.
33 M. Thongngam, S. Viturat, N. Lumdubwong, W. Zhou and U. Klinkesorn, Ultrasound-assisted formation of chitosan-glucose Maillard reaction products to fabricate nanoparticles with enhanced antioxidant activity, *Ultrason. Sonochem.*, 2023, **97**, 106466.
34 B. Li, G. Sun, J. Ran, X. Shen and H. Tong, Three-dimensional hierarchical porous carbon/graphene composites derived from graphene oxide-chitosan hydrogels for high performance supercapacitors, *Electrochim. Acta*, 2015, **171**, 13–22.
35 X. Xu, L. Szabó, K. Uto, J. Henzie, Y. Yamauchi, I. Ichinose and M. Ebara, Tailoring the Structure of Chitosan-Based Porous Carbon Nanofiber Architectures toward Efficient Capacitive Charge Storage and Capacitive Deionization, *ACS Appl. Mater. Interfaces*, 2022, **14**, 4004–4021.
36 C. Zhang, W. Zhu, J. Lin, S. Pan, Q. Wang, N. Liao, P. Yu and M. Zhang, Flexible Strain Sensor Based on Copper/Graphene Composite Films, *ACS Appl. Nano Mater.*, 2024, **7**, 358–369.
37 Y. Wu, T. Yan, J. Tang and Z. Pan, Highly sensitive strain sensor with wide strain range fabricated using carbonized natural wrapping yarns, *Mater. Res. Bull.*, 2021, **143**, 111452.
38 G. Shen, X. He, J. Liang, Z. Liu, Y. Xin, T. Liang, J. He, C. Zhang, Y. Chen and X. He, Stretchable Strain Sensors Based on Two- and Three-Dimensional Carbonized Cotton Fabrics for the Detection of Full Range of Human Motions, *ACS Appl. Electron. Mater.*, 2021, **3**, 3287–3295.
39 Z. Liu, L. Xu, H. Zhai, X. Chen, R. Sun, S. Lyu, Y. Fan, Y. Yi, Z. Chen, L. Jin, J. Zhang, Y. Li and T. T. Ye, Moisture-Resilient Graphene-Dyed Wool Fabric for Strain Sensing, *ACS Appl. Mater. Interfaces*, 2020, **12**, 13265–13274.
40 J. Wang, C. Yan, W. Kang, M. Cui, X. Wang, C. Y. Foo, K. J. Chee and P. S. Lee, Highly Stretchable Piezoresistive Graphene–Nanocellulose Nanopaper for Strain Sensors, *Adv. Mater.*, 2013, **26**, 2022–2027.
41 H. Tian, Y. Pang, L. Tao, Y. Li, X. Wang, N. Deng, Y. Yang and T.-L. Ren, Flexible, Highly Sensitive, and Wearable Pressure and Strain Sensors with Graphene Porous Network Structure, *ACS Appl. Mater. Interfaces*, 2016, **8**, 26458–26462.
42 J. Chen, Q. Liu, Y. Li and G. Shi, High-Performance Strain Sensors with Fish-Scale-Like Graphene-Sensing Layers for Full-Range Detection of Human Motions, *ACS Nano*, 2016, **10**, 7901–7906.
43 Y. Liu, C. Gao, F. Gu, Z. Chen, Z. Su, H. Du, D. Xu, K. Liu and W. Xu, Biodegradable Ecoflex encapsulated bacterial cellulose/polypyrrole strain sensor detects motion with high sensitivity, flexibility and scalability, *Chem. Eng. J.*, 2023, **460**, 141769.
44 X. Meng, T. Sun, L. Liu, C. Zhang, H. Zhao, D. Wang, J. Zhang, S. Niu, Z. Han and L. Ren, Flexible Equivalent Strain Sensor with Ordered Concentric Circular Curved Cracks Inspired by Scorpion, *ACS Appl. Mater. Interfaces*, 2022, **14**, 29441–29450.
45 W. Wang, L. Lu, X. Lu, Z. Liang, H. Lin, Z. Li, X. Wu, L. Lin and Y. Xie, Scorpion-inspired dual-bionic, microcrack-assisted wrinkle based laser induced graphene-silver strain sensor with high sensitivity and broad working range for wireless health monitoring system, *Nano Res.*, 2023, **16**, 1228–1241.
46 B. L. Zambrano, S. A. Dual, S. Sündermann, N. Cesarovic, M. Kron, K. Magkoutas, J. Hengsteler, V. Falk, C. Starck, M. Meboldt, J. Vörös and M. S. Daners, Continuous Heart Volume Monitoring by Fully Implantable Soft Strain Sensor, *Adv. Healthcare Mater.*, 2020, **9**, 2000855.